J Mater Sci (2018) 53:4010–4021

Ceramics

Effects of VC additives on densification and elastic and mechanical properties of hot-pressed ZrB_2–SiC composites

Shuqi Guo[1,*]

[1] Research Center for Structural Materials, National Institute for Materials Science, 1-2-1 Sengen, Tsukuba, Ibaraki 305-0047, Japan

Received: 8 August 2017
Accepted: 21 November 2017
Published online: 28 November 2017

ABSTRACT

In this study, highly dense ZrB_2-20 vol% SiC composites with 3–10 wt% VC additives were prepared by hot-pressing at 1750 °C for 1 h under a pressure of 20 MPa in a vacuum. The densification behavior and elastic and mechanical properties of the obtained composites were examined, and the effect of the VC content on the densification and the properties is analyzed. The addition of VC promotes the activation of densification mechanism at a lower temperature and inhibits the growth of ZrB_2 and SiC grains during the sintering. In addition, the elastic moduli, hardness and fracture toughness that measured in the obtained composites are constant and independent of the VC content, with a shear modulus of ~ 220 GPa, Young's modulus of ~ 500 GPa, hardness of ~ 20 GPa and fracture toughness of ~ 4.4 MPa $m^{1/2}$. On the other hand, the flexural strength of the composites decreased as the VC content increased from 3 to 7 wt% and then it increased with further increasing the VC content to 10 wt%, with strength values of 620–770 MPa.

Introduction

Zirconium diboride (ZrB_2) is a refractory transition-metal diboride composed of elements from the fourth to sixth groups of the periodic table. Most of these diborides have melting points greater than 3000 °C, high thermal and electrical conductivities, chemical inertness against molten metals and good thermal shock resistance, making them potential candidates for several high-temperature structural applications [1–3]. The major problems of ZrB_2 ceramics involve sinterability [4] and high-temperature oxidation [5, 6]. Because of strong covalent bonds and low self-diffusivity [4], the densification of ZrB_2 powder requires very high temperatures (> 2100 °C) and external pressure (≥ 20 MPa). In addition, it is known that heating single-phase ZrB_2 ceramics in air or oxidized atmosphere produces a scale composed of ZrO_2 and B_2O_3 in which B_2O_3 has a high vapor pressure and is vaporized above 1300 °C [5, 6].

Overcoming poor sinterability and poor oxidation resistance requires sintering activator and protective borosilicate glass scale formed on the surface of ceramics. One of the most promising solutions for

Address correspondence to E-mail: GUO.Shuqi@nims.go.jp

https://doi.org/10.1007/s10853-017-1850-7

improving sinterability as well as for improving oxidation resistance of ZrB_2 ceramics is to apply secondary phase to the ZrB_2 ceramics for obtaining a multiple-phases ceramic composite. It is known that SiC-containing ZrB_2 ceramic composite showed improvement of sinterability and better oxidation resistance [7–13]. Recently, this composite has become a strong potential candidate for a variety of high-temperature structural applications. The addition of SiC is believed to produce an intergranular liquid phase that aids the densification of ZrB_2 [7–12]. In addition, the improvement of oxidation resistance due to the addition of SiC is thought to arise from the formation of a coherent passivating oxide scale on the surface [11–13]. Furthermore, the presence of SiC limits the grain growth of ZrB_2 during the sintering [8–10], leading to a higher strength. Nevertheless, a sintering temperature of equal to or above 1900 °C is still required to obtain highly dense ZrB_2–SiC ceramic composites. In an attempt to further lower the densification temperature of ZrB_2–SiC composite, $MoSi_2$ has been added to aid the densification. The study shows that densities exceeding 97% were obtained for 5 and 10 vol% SiC-containing ZrB_2 powders at 1800 °C for 30 min under a pressure of 30 MPa in a vacuum by the addition of 20 vol% $MoSi_2$ [14, 15]; however, density of ~ 94% was obtained as 20 vol% SiC was added to ZrB_2 powder. In addition, recent studies of ZrB_2–SiC ceramics with 1–5 wt% AlN or SiAlON additives showed that highly dense ceramics were obtained by hot-pressing under a low pressure of 10 MPa or pressureless sintering processes at 1900 °C for 2 h, as a result of the liquid phase formation during the sintering [16, 17].

On the other hand, previous study of ZrB_2-based ceramics showed that groups IV–VI transition-metal carbides could be used as a sintering activator to promote densification of ZrB_2–SiC composites at lower temperature [18]. Grigoriev et al. [19] showed when Cr_3C_2 was used as a sintering activator, highly dense ZrB_2 ceramic was obtained by hot-pressing at different temperatures between 1500 and 1750 °C, dependent on the Cr_3C_2 content. Zou et al. [20] showed that highly dense ZrB_2–SiC composites with VC additives could be prepared by pressureless sintering at or above 2000 °C for 2 h in Ar, dependent on the VC content. In addition, they showed that density exceeding 99% was obtained at 1900 °C for 1 h under a pressure of 30 MPa in Ar for ZrB_2–SiC-VC powder using high-energy ball milling, followed by hot-pressing [21]. However, the effects of VC content on densification behavior, elastic and mechanical properties of the ZrB_2–SiC composites with VC additives are not well understood. Furthermore, very recently, studies of ZrB_2–SiC composites with 5 vol% WC showed that highly dense composites were obtained by hot-pressing or spark plasma sintering at or above 1950 °C [22, 23]; this suggests that WC should be a potential sintering aid for ZrB_2–SiC ceramics.

In this study, four compositions ZrB_2–SiC composites with VC additives were prepared by hot-pressing at 1750 °C for 1 h under a pressure of 20 MPa in a vacuum. The densification behavior that occurred during the sintering and the microstructure of the obtained composites were examined. The elastic and mechanical properties of the composites were measured at room temperature. The effect of VC content on the densification behavior, elastic and mechanical properties was analyzed.

Experimental procedure

Starting powder

The starting powders used in this study were: ZrB_2 powder (d_{50} = 2.1 μm, Grade F, Japan New Metals, Osaka, Japan), α-SiC (d_{50} = 0.5 μm, UF-15, H.C. Starck, Berlin, Germany) and VC powder (d_{50} = 1.8 μm, Japan New Metals, Osaka, Japan). Four compositions of 3, 5, 7 and 10 wt% VC-containing ZrB_2-20 vol% SiC composites were prepared to examine the effect of VC content on the densification, and elastic and mechanical properties. Hereafter, the four ZrB_2–SiC composites with the VC additives are denoted as ZSVC03, ZSVC05, ZSVC07, and ZSVC10 (Table 1), respectively. In order to obtain homogeneous powder mixtures as well as to reduce starting powder particles size, the VC-doped ZrB_2–SiC powder mixtures were ball-milled using SiC milling media and ethanol for 24 h; subsequently the resulting slurry was dried. Before being sintered, the dried powders were sieved through a metallic sieve with 60-mesh screen size.

Hot-pressing

The obtained powders mixtures were consolidated by hot-pressing in a graphite die lined with graphite foil in tablets 21 mm × 25 mm × 3.0 mm in size.

Table 1 Compositions, densities, average grain size of ZrB_2 and SiC and phase composition of the composites as determined by X-ray diffraction

Materials	Compositions (wt%)			Grain diameter, d (μm)		Bulk density (g/cm^3)	Relative density (%TD)	Primary phase	Secondary phase
	ZrB_2	SiC	VC	ZrB_2	SiC				
ZSVC03	85.25	11.75	3	2.12 ± 0.92	1.94 ± 0.71	5.46	99.1	ZrB_2	SiC, V_3B_4, ZrC
ZSVC05	83.25	11.75	5	2.17 ± 0.96	1.83 ± 0.69	5.44	98.6	ZrB_2	SiC, V_3B_4, ZrC
ZSVC07	81.24	11.76	7	2.13 ± 0.91	1.61 ± 0.65	5.44	98.8	ZrB_2	SiC, V_3B_4, ZrC
ZSVC10	78.22	11.78	10	2.14 ± 0.89	1.46 ± 0.38	5.45	98.9	ZrB_2	SiC, V_3B_4, ZrC

Powder compacts were heated to 1750 °C with a heating rate of ~ 15 °C/min in a vacuum. When the die temperature reached 1750 °C, a uniaxial pressure of 20 MPa was applied. After hot-pressing at 1750 °C for 60 min, the pressure load was removed and the temperature was decreased to 500 °C with a heating rate of ~ 15 °C/min, and then the sample was cooled to room temperature in the furnace. In addition, several samples were heated to 1750 °C with ~ 15 °C/min under a pressure of 20 MPa in a vacuum with subsequent isothermal heating of 60 min to examine the densification behavior that occurred during the sintering in detail. During the entire sintering process, the changes in temperature and displacement along the pressure direction were recorded on a computer to monitor the densification behavior. The densities of the obtained composites were measured from Archimedes method with distilled water as the medium.

Characterizations

X-ray diffraction (XRD, SmartLab, Rigaku, Co., Tokyo, Japan) was used to identify any crystalline phases present in the prepared composites. The microstructure of the composites was characterized by field emission scanning electron microscopy (SEM, QUANTA-200F, FEI Company, Hillsboro, OR, USA). The grain size, d, of ZrB_2 and SiC in the composites was determined by measuring the average linear intercept length, d_m, of the grains in SEM images of the composites, according to the relationship of $d = 1.56d_m$ [24]. In addition, the shear modulus, G, Young's modulus, E, bulk modulus, B and Poisson's ratio, ν, of the composites were calculated using the longitudinal and transverse soundwave velocities that were measured in the specimens with ultrasonic equipment (TDS 3052B, Tektronix Inc. Beaverton, OR USA). The detailed calculations are reported elsewhere [25]. The hardness, H_v, and the fracture toughness, K_{IC}, of the composites were determined using an indentation crack size measurement. The indentation tests were performed on the polished surface of the specimens by loading with a Vickers indenter (AVK-A, Akashi, Co., Ltd., Yokohama, Japan) for 15 s in ambient air at room temperature. The corresponding diagonals of the indentation and crack sizes were measured using an optical microscope attached to the indenter. An indentation load of 98 N was applied, and ten indents were made for each measurement. The fracture toughness of the composites was calculated from the Anstis equation [26].

Specimens, averaging 25 mm × 2.5 mm × 2 mm in size, were cut from the hot-pressed composites plates, by using a diamond grinder. The surfaces of the specimens were ground with an 800-grit diamond wheel and then one of the large surfaces was polished with diamond paste down to 1.0 μm. The flexural strength of the specimens was measured using a four-point bending test fixture (inner span 10 mm and outer span 20 mm) at room temperature. The polished surface of the specimen was used as the tensile surface for the bending test. The bending test was carried out using an Autograph testing system (AG-50KNI, Shimadzu, Kyoto, Japan) with a crosshead speed of 0.5 mm/min. A minimum of five specimens were used for each measurement. After fracture, the fracture surfaces were observed using SEM.

Results and discussion

Densification and microstructure

Figure 1 presents the shrinkage curves obtained during the hot-pressing cycles for the four

compositions samples. The four composites exhibited similar shrinkage curves; however, the shrinkage occurred at different temperatures, dependent on the VC content. The onset temperature of densification was identified to be as: ~ 1560 °C for ZSVC03, ~ 1530 °C for ZSVC05, ~ 1510 °C for ZSVC07, and ~ 1490 °C for ZSVC10. It is evident that the onset temperature of densification lowered as the VC content increased. The onset temperature of densification was lower than that of ZrB_2-20 vol% SiC powder with 4 vol% Si_3N_4 additives [27] and was almost the same as that observed during the spark plasma sintering of ZrB_2-20 vol% SiC ceramic [10]. Thus, the addition of VC to ZrB_2–SiC powder led to activation of the densification mechanism at a lower temperature. Beyond the onset temperature of densification, the shrinkage continuously progressed with further increasing temperature. Unlike the onset temperature of densification, the maximum shrinkage rate was nearly same for the four composites, regardless of the VC content. When the heating to 1750 °C ended, the densification was not completed for all instances. During subsequent isothermal heating, the shrinkage continued until the end of the 60-min holding time for the four compositions.

The densities measured in the hot-pressed ZrB_2-20 vol% SiC composites with VC additives are summarized in Table 1. Densities exceeding 98% were obtained for the four composites after the hot-pressing at 1750 °C for 60 min under a pressure of 20 MPa in a vacuum. Previously studies of ZrB_2–SiC composites showed that the highly dense composites were obtained at 1900 °C by hot-pressing and/or spark plasma sintering [10, 12] although their onset temperatures of densification are approximately identical. In addition, for ZrB_2-20 vol% SiC composites with 4 vol% Si_3N_4 additives, density of approximately 98% was obtained at 1800 °C under an applied pressure of 30 MPa by hot-pressing [27]. Previous study of Al_2O_3 ceramics showed that a higher load applied during the sintering enhanced the densification at a lower temperature [28]. Thereby, these comparisons indicate that the addition of VC substantially accelerated the densification of ZrB_2–SiC composites during the sintering at a lower temperature, suggesting that VC is an effective sintering activator for ZrB_2–SiC system.

It is known that the improvement of densification due to additives such as carbides, nitrides and disilicide is attributable to the removal of oxygen impurities present in the starting powders or to the formation of an intergranular liquid phase that favors the process of grain rearrangement and improves the packing density of the particles [29]. Previous studies of ZrB_2–SiC-VC system showed that the addition of VC to ZrB_2–SiC led to the removal of ZrO_2 through the following reaction (1) [18, 20, 21], therefore densification.

$$ZrO_2(s) + 3VC(s) \rightarrow ZrC(s) + 3V(s) + 2CO(g) \quad (1)$$

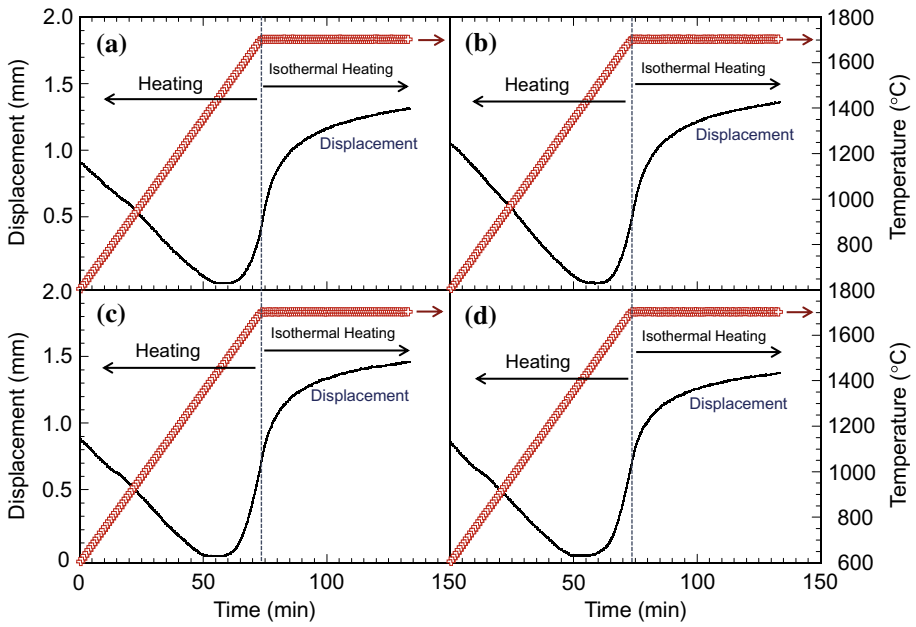

Figure 1 Shrinkage curves obtained during the hot-pressing cycles at 1750 °C for the four composites: **a** ZSVC03, **b** ZSVC05, **c** ZSVC07 and **d** ZSVC10.

According to Eq. (1), it could be found that single-phase V could be present during the occurrence of the reaction of ZrO_2 with VC. In addition, the non-stoichiometric VC_x ($x < 1$) compound was determined as an intermediate phase by XRD in ZrB_2–SiC-VC during sintering [21], as a result of the dissociation of VC [18]. On the basis of the V–C phase diagram, thus it seems to be expected the presence of the eutectic phases of VC_x–V which melting point is equal to be ~ 1650 °C during the sintering. Presumably, the improvement of densification in the ZrB_2-20 vol% SiC composites with VC additives is attributable to the removal of oxygen impurities and the formation of the eutectic liquid phase with a lower melting point.

Figure 2 displays the XRD patterns of the hot-pressed ZrB_2-20 vol% SiC composites with VC additives. The ZrB_2, SiC, ZrC, and V_3B_4 phases were detected in each instance, with no VC phase. The ZrB_2 phase is the primary phase; other phases are the secondary phase. The presence of the V_3B_4 and ZrC phases indicates that the reaction between VC and ZrB_2 occurred during the sintering. The absence of VC phase suggests that VC was completely consumed to form new refractory phases such as ZrC and V_3B_4 during the sintering. Similar reaction products were found in ZrB_2-VC ceramics sintered at 1650 °C in vacuum for 1 h [21]. For ZrB_2-VC or ZrB_2–SiC-VC composites sintered at 1900 °C in vacuum for 1 h [21], however, VB_2 phase was detected, with no V_3B_4 phase. The disappearance of V_3B_4 phase suggests that the reaction of ZrB_2 with VC is dependent on sintering temperature. In addition, the peak intensity of the ZrB_2 phase decreased as the VC content increased, while the peak intensities of the ZrC and V_3B_4 phases intensified. The enhancement of the peak intensities with the VC content suggests that the ZrC and V_3B_4 phases formed during the sintering increased as the VC content increased. Unlike the ZrB_2 and VC, the peak intensity of the SiC phase remained nearly constant, regardless of the VC content. In addition, there was no evidence for the occurrence of reaction between VC and SiC during the sintering (Fig. 2). These XRD results suggest that VC preferentially reacts with the ZrB_2 phase, rather than the SiC phase, during the sintering at 1750 °C. The phase compositions determined by XRD for the hot-pressed composites are summarized in Table 1. Because the VC replaced with the ZrC and V_3B_4 after

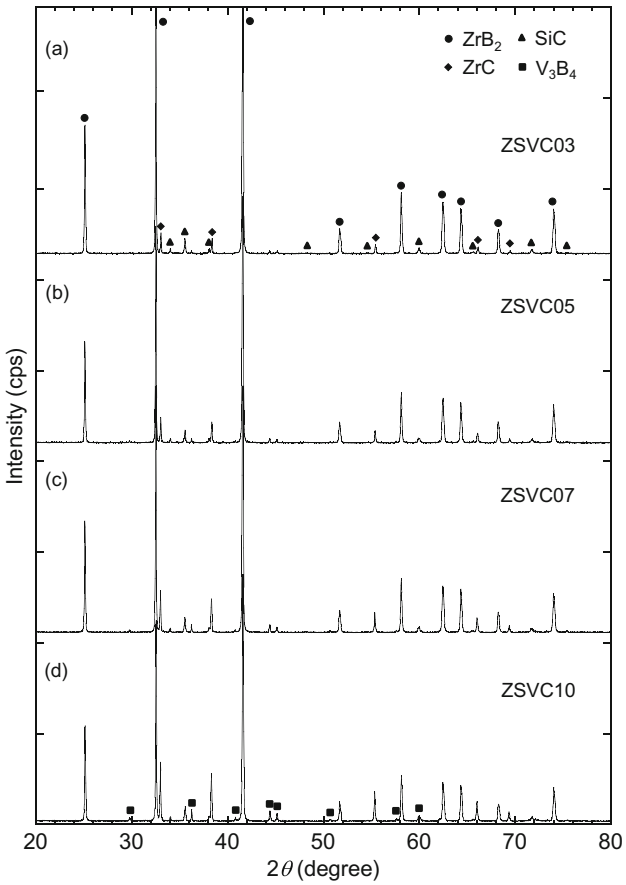

Figure 2 XRD patters of the four composites: **a** ZSVC03, **b** ZSVC05, **c** ZSVC07 and **d** ZSVC10.

the sintering by the reaction of VC with ZrB_2 (Fig. 2), thus the oxidation resistance of the composites seems to be improved [30] compared to ZrB_2–SiC composite, a further detailed investigation of the oxidation behavior is clearly needed.

In Fig. 3, backscattered electron (BSE) SEM micrographs of the microstructures of the four composites are presented. The general microstructures of the four composites are similar in the morphology. The composite microstructures consist of the equiaxed ZrB_2 (gray contrast), finer SiC (dark contrast), ZrC (white–gray contrast) and irregularly coarsened V_3B_4 (dark-gray contrast) grains. The ZrC phase formed during the sintering did not surround the ZrB_2 particles, and it is present at the ZrB_2 grains-boundaries and/or ZrB_2 and SiC grains-boundaries. Because of the formation of the eutectic liquid phases between the ZrB_2 and the VC during the sintering, thus it seems to be reasonable that the presence of the liquid phase led to moving of the ZrC particles formed due to the reaction of ZrB_2 with VC toward other grain

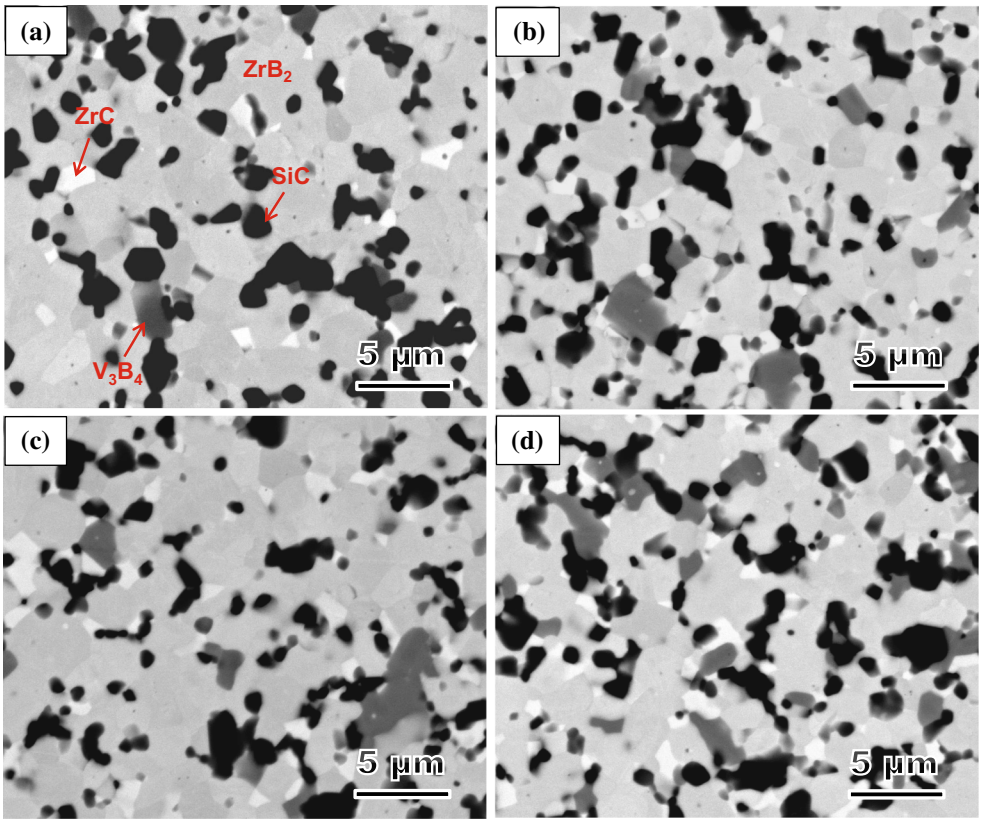

Figure 3 BSE–SEM images of microstructures of the four composites: **a** ZSVC03, **b** ZSVC05, **c** ZSVC07 and **d** ZSVC10.

boundaries. Similar behavior was reported in hot-pressed ZrB_2-40 vol% B_4C composite [31]. In addition, the amount of V_3B_4 and ZrC phases that formed during sintering increased as the VC content increased, with a significant increase observed in ZSVC07 and ZSVC10. These observations are agreement with the XRD patterns obtained in the four composites (Fig. 2).

Moreover, the microstructures of the composites were observed under the secondary electron (SE) image; the SE-SEM micrographs are shown in Fig. 4. Combining Fig. 4 with Fig. 3, it is found that the SiC grains are very fine and they became gradually finer with increase in the VC content (Table 1). However, the ZrB_2 grains are larger and their size remained nearly constant, regardless of the VC content (Table 1). The grain sizes of ZrB_2 and SiC are similar to those reported in ZrB_2-20 vol% SiC with 5 vol% VC additives hot-pressed at 1900 °C in vacuum for 1 h [21]. In comparison, previous studies of ZrB_2-20 vol% SiC with 5 vol% Yb_2O_3 additives showed that ZrB_2 and SiC grains in starting powder grew from 2 and 0.7 μm, respectively, to ~ 10 and ~ 3.9 μm after hot-pressing at 1850 °C for 60 min [32] and to ~ 4.5 and ~ 2.1 μm after spark plasma sintering at 1900 °C for 4 min [33]. These comparisons indicate that the addition of VC inhibited the coarseness of the ZrB_2 and SiC grains during the sintering, and this inhibiting effect on the grain growth is more effective for ZrB_2 grains than for SiC grains. However, trace quantities of smaller porosities were found at the grains-boundaries for the four composites (indicated by arrows in Fig. 4). The formation of the porosities was previously reported in hot-pressed ZrB_2-40 vol% B_4C composite by Nayebi et al. [31] who showed that the porosities were formed due to the releasing of gaseous phases and the diffusion C or B atoms from B_4C toward ZrB_2 particles during the sintering when the reaction of ZrO_2 with B_4C occurred. Similar cause, although not well known, could be expected in the ZrB_2–SiC-VC ceramics investigated in this study because of the occurrence of CO gas through Eq. (1) and the diffusion of C atom toward ZrB_2 particles during the sintering.

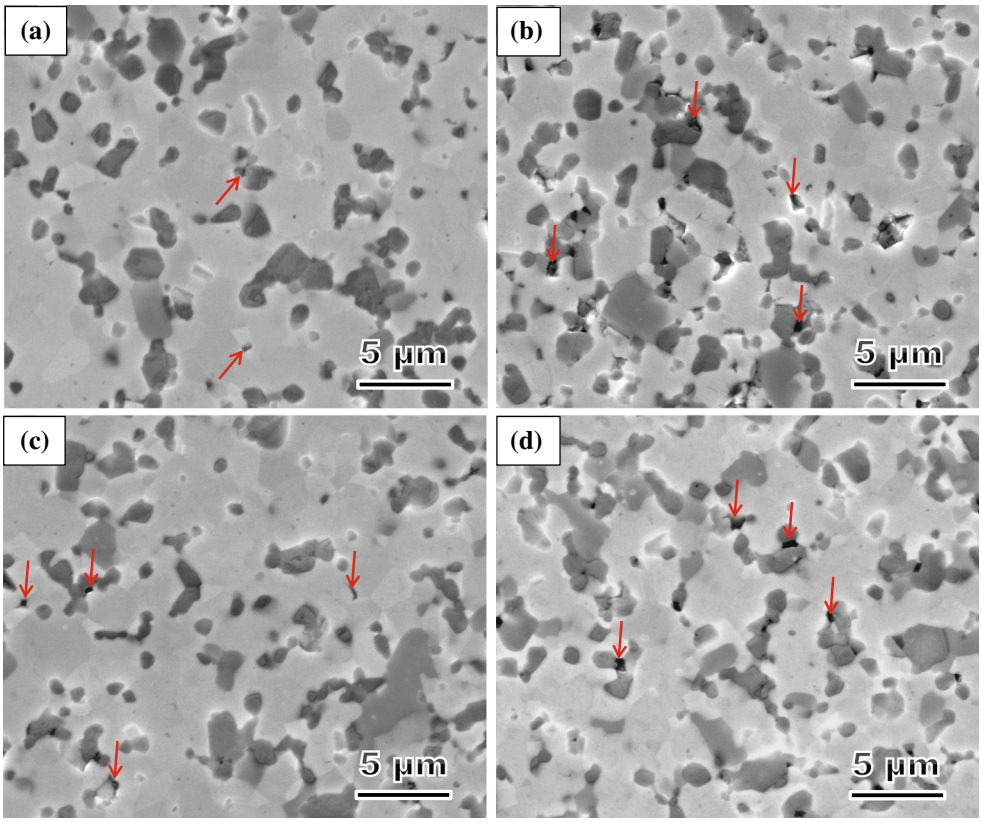

Figure 4 SE-SEM images of microstructures of the four composites: **a** ZSVC03, **b** ZSVC05, **c** ZSVC07 and **d** ZSVC10. These images corresponded to the images in Fig. 3, respectively.

Elastic and mechanical properties

Elastic moduli, hardness and fracture toughness

Table 2 summarizes the elastic moduli, hardness and fracture toughness of the four composites. The shear modulus, Young's modulus and bulk modulus measured in the four composites remain nearly constant, regardless of the VC content. Accordingly, the addition of 3–10 wt% VC did not substantially affect these moduli. Additionally, the Poisson's ratio value for each of the four composites is the same and independent of the VC content. The elastic moduli of the four composites are comparable to or greater than those of ZrB_2 ceramics and/or ZrB_2–SiC composites [34–36]. In addition, the hardness and the fracture toughness of the four composites are nearly same (Table 2), with a hardness of ~ 20 GPa and a fracture toughness of ~ 4.4 MPa $m^{1/2}$. The hardness is lower than that of ZrB_2–SiC (10–30 vol% SiC) composites (H_v = 24 GPa) [35], but it is comparable to that of ZrB_2–ZrC–SiC system (H_v = 19–22 GPa) [36] and is greater than that of ZrB_2-20 vol% SiC composite with 5 vol% VC hot-pressed at 1900 °C in vacuum for 1 h (H_v = 18 GPa) [21]. The fracture toughness of the composites is comparable to that of ZrB_2–SiC (10–30 vol% SiC) composites (K_{IC} = 4.1–5.3 MPa $m^{1/2}$) [35] as well as to that of ZrB_2-20 vol% SiC composites with 5 vol% VC hot-pressed at 1900 °C in vacuum for 1 h (K_{IC} = 4.4–5.5 MPa $m^{1/2}$) [21]. However, the fracture toughness of the composites is lower than that of ZrB_2–ZrC–SiC system (K_{IC} = 4.6–6.1 MPa $m^{1/2}$) [36].

The crack propagation behavior of the four composites was observed under SEM imaging of Vickers indentation cracks in each sample; a typical cracking pattern is shown in Fig. 5. As is evident in this figure, the crack propagated across the many ZrB_2 grains; the crack deflection occurred at the ZrB_2/SiC, ZrB_2/V_3B_4, ZrB_2/ZrC grain boundaries and some ZrB_2 grain boundaries. The SiC, V_3B_4, ZrC and ZrB_2 grain bridging behavior is observed during the crack propagation path. This crack propagation behavior was observed in each instance, regardless of the VC content. The crack propagation behavior observed in the composites is most likely controlled by the complex residual stresses state that developed during

Table 2 Shear modulus, Young's modulus, Bulk modulus, Poisson's ratio, hardness, fracture toughness and flexural strength of the hot-pressed composites

Materials	Elastic properties				Hardness H_v (GPa)	Fracture toughness K_{IC} (MPa $m^{1/2}$)	Flexural strength σ_{fs} (MPa)
	G (GPa)	E (GPa)	B (GPa)	v			
ZSVC03	225	512	237	0.14	19.8 ± 1.6	4.4 ± 0.2	687.9 ± 93.8
ZSVC05	222	505	234	0.14	20.9 ± 1.0	4.3 ± 0.3	672.7 ± 60.8
ZSVC07	219	499	231	0.14	21.3 ± 0.8	4.3 ± 0.3	621.2 ± 37.1
ZSVC10	217	494	228	0.14	19.8 ± 1.3	4.4 ± 0.5	771.1 ± 148.7

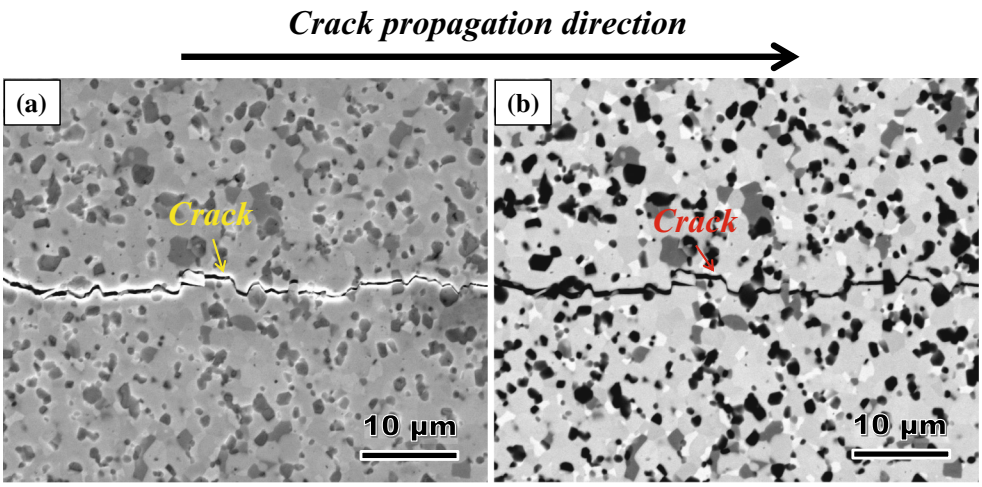

Figure 5 Typical crack propagation behavior in ZSVC07: **a** SE-SEM image and **b** corresponding BSE–SEM image.

cooling from the processing temperature due to the thermal expansion mismatch among ZrB_2, SiC, ZrC and V_3B_4. It is known that the coefficient of thermal expansion (CTE) of ZrB_2 is ~ 8.3 ppm/K which is larger than that of SiC (~ 4 ppm/K), ZrC (~ 5.2 ppm/K) and V_3B_4 (~ 7.6 ppm/K, assuming that the CTE of V_3B_4 is the same as VB_2). Thus, the thermal expansion mismatch between ZrB_2 and SiC or ZrB_2 and ZrC or ZrB_2 and V_3B_4 induced the residual compressive stresses surround SiC, ZrC and V_3B_4 on cooling from the processing temperature to room temperature. The residual compressive stresses led to the crack deflection at the ZrB_2/SiC, ZrB_2/V_3B_4, ZrB_2/ZrC interface. Similar crack propagation behavior has been reported for ZrB_2–SiC composites [9]. The same crack propagation behavior observed in the four composites suggests that the same toughening mechanisms, including crack deflection, grain pullout, elastic bridging and frictional grain bridging, are operated in these materials. Because the four composites have similar microstructural morphology (Figs. 3 and 4), with no substantial differences in the grain sizes (Table 1), consequently the fracture toughness is nearly constant for these composites and independent of the VC content.

Flexural strength

The room temperature four-point flexural strengths measured in the four composition composites are summarized in Table 2. Unlike the elastic moduli, hardness and fracture toughness, the flexural strengths that were obtained from the four composites and the scattering of strengths are substantially related to the VC content, with strength values of 620–770 MPa. The maximum strength was observed in ZSVC10, while the minimum strength was obtained in ZSVC07. The strength values displayed by the four composites are comparable or greater than those for the single-phase ZrB_2 ceramics or ZrB_2-20 vol% SiC composites consolidated by hot-pressing [12, 27, 33]. In addition, these strengths are

comparable to three-point flexural strengths of ZrB_2-20 vol% SiC composites with 5 vol% VC hot-pressed at 1900 °C in vacuum for 1 h (σ_{fs} = 610–804 MPa) [21].

To examine the fracture origin of material, SEM observations were performed on the fracture surfaces of specimens; typical SE-SEM micrographs are shown in Fig. 6. As is evident in this figure, the fracture origin is located at the defects in the surfaces (indicated by arrows in Fig. 6). Presumably, the major cause of failure was the presence of the defects in the surfaces. In addition, the defects observed on the fracture surfaces are larger for ZSVC07 than for ZSVC05. Thus, the low flexural strength observed in ZSVC07 is a result of the larger defects present in the composite, while the small scattering of strength

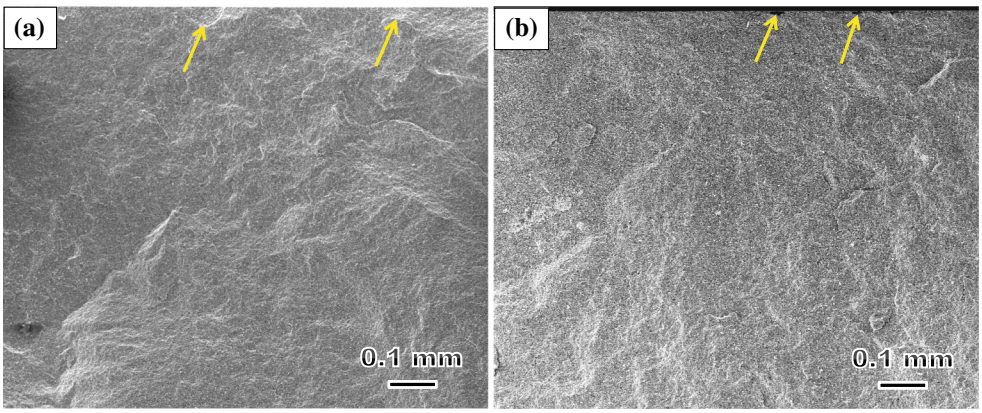

Figure 6 SE-SEM images of fracture surfaces of the composites: **a** ZSVC05 and **b** ZSVC07. These images show origination of fracture from the defects in the surfaces of specimens.

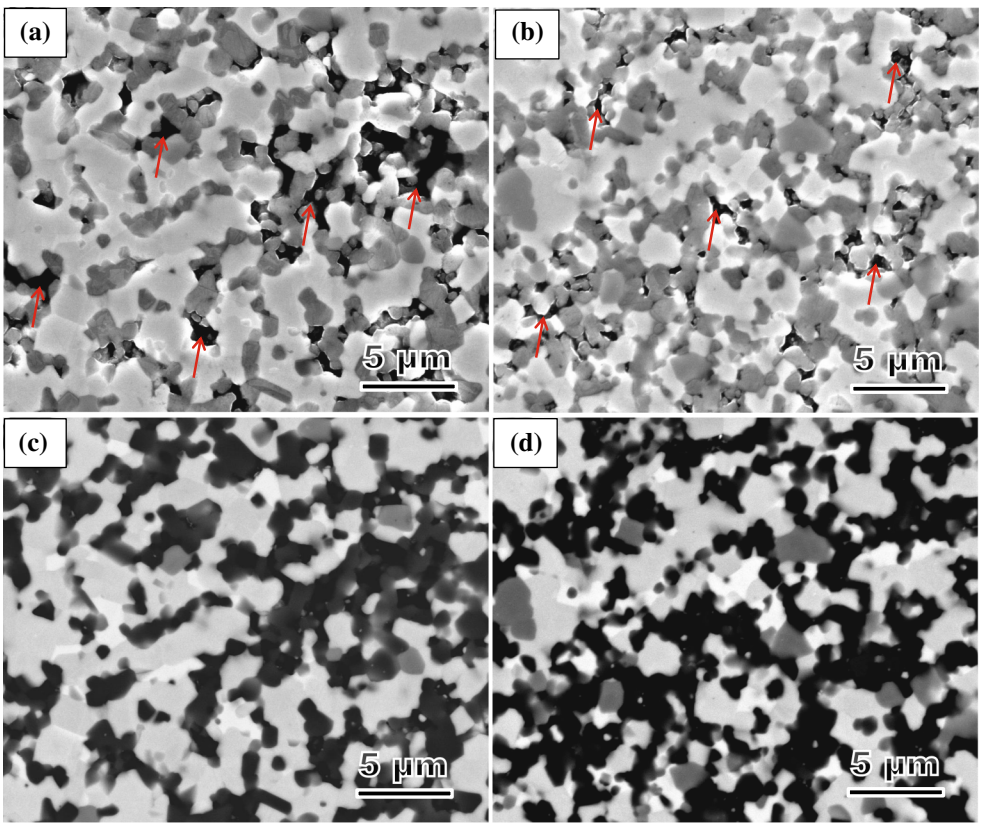

Figure 7 SE-SEM images of defects in **a** ZSVC03 and **b** ZSVC07, **c** and **d** corresponding BSE–SEM images.

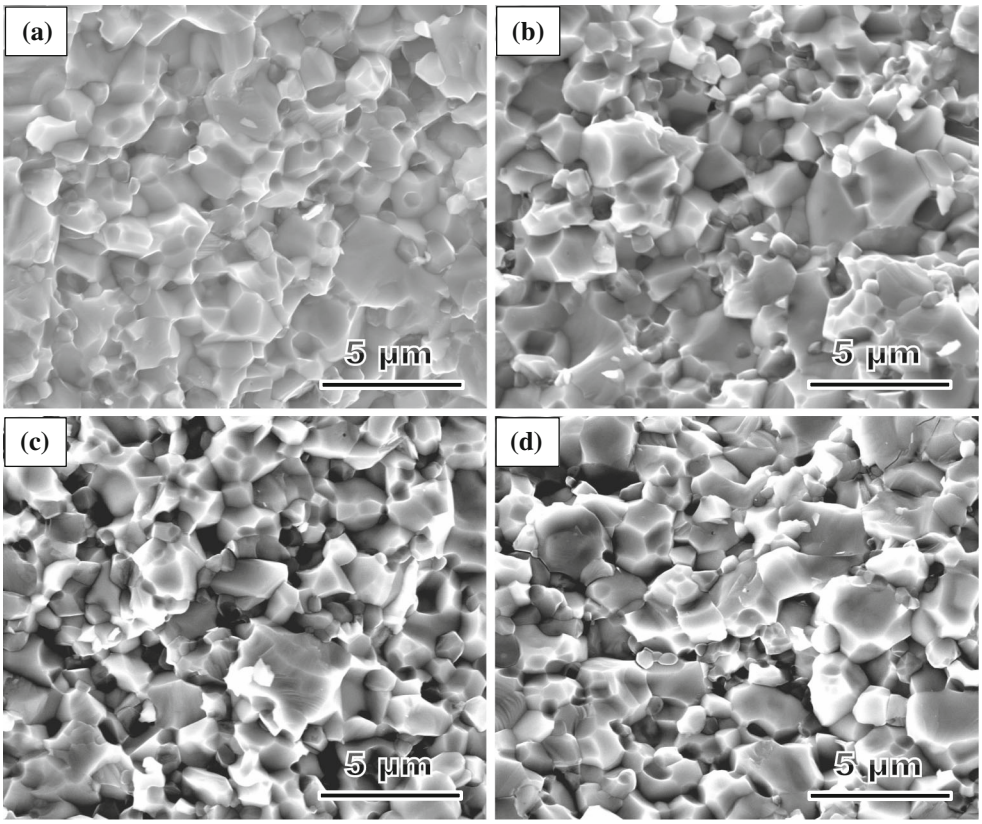

Figure 8 SE-SEM images of fracture surfaces of the four composites: **a** ZSVC03, **b** ZSVC05, **c** ZSVC07 and **d** ZSVC10.

(Table 2) suggests that the defects sizes have narrow distribution. In contrast, the higher strength and larger scattering of strength for ZSVC10 suggest that the presence of smaller-sized defects with widely size distribution in the composites.

Further SE-SEM observations of the microstructures of the composites show that the defects contain many larger pores (indicated by arrows in Fig. 7a, b). In addition, the corresponding BSE–SEM images show that the V_3B_4 (dark-gray contrast) and/or ZrC (white contrast) phase are more in the defect zones (Fig. 7c, d) than in the non-defect zones (Fig. 3a, c). These observations indicate that the defects in the surface were the larger pore-containing agglomerates of the sintering phases formed during the sintering. These larger porous agglomerates of the sintering phases were probably traces of the blocks of the eutectic liquid phase, produced due to the reaction between the ZrB_2 and VC during the sintering. Because the formation of a large number of V_3B_4 and ZrC consumed the eutectic liquid phases during the sintering, this makes densification difficult at 1750 °C; therefore, large porous agglomerates of the sintering phases are formed.

Figure 8 presents FE-SEM micrographs of the fracture surfaces for the four composites. The fracture surfaces of ZSVC03 are relatively flat (Fig. 8a), with a transgranular fracture for ZrB_2 and intergranular fracture for SiC, V_3B_4 and ZrC phases. The fracture surfaces became rough as the VC content increased (Fig. 8b–d) because the amount of V_3B_4 and ZrC increased and the amount of ZrB_2 decreased accompanying increase in the VC content. In particular, for ZSVC07 and ZSVC10, their fracture surfaces are significantly rough, with protruding a number of fine grains and open sockets left by grain pullout. For comparison, previous studies in hot-pressed ZrB_2 or ZrB_2–SiC composites showed that their fracture surfaces are relatively flat with a transgranular fracture characterization [12, 27, 33]. This difference indicates that the intergranular fracture is more easily to occur for ZrB_2–SiC composites with VC additives compared to ZrB_2–SiC ones without VC additives. The different fracture behavior due to VC addition may be associated with the following two factors: (1) weak

intergranular bonding due to VC addition accompanying the formation of V_3B_4 and ZrC at the grain boundaries during the sintering, and (2) the complex residual stress state that develops during cooling from the processing temperature due to the presence of the new V_3B_4 and ZrC phases.

Conclusions

Four ZrB_2-20 vol% SiC composites with 3–10 wt% VC additives were prepared by hot-pressing at 1750 °C for 1 h under a pressure of 20 MPa in a vacuum. The densification behavior, microstructure and elastic and mechanical properties of the obtained composites were examined. The major results are summarized below.

1. Highly dense ZrB_2-20 vol% SiC-based composites with 3–10 wt% VC additives were obtained by hot-pressing at 1750 °C for a holding time of 1 h under a pressure of 20 MPa in a vacuum, regardless of the VC content.
2. The obtained composites comprised ZrB_2, SiC, V_3B_4 and ZrC phases, with no VC phase. The addition of VC significantly inhibited the growth of ZrB_2 and SiC grains during the sintering.
3. The Young's modulus, shear modulus, bulk modulus and Poisson's ratio of the composites remained constant, regardless of the VC content, and their values were as follows: $E = 500$ GPa, $G = 220$ GPa, $B = 230$ GPa, and $\nu = 0.14$. Also, the hardness and fracture toughness of the composites were constant and independent of the VC content, with a value of $H_v = 20$ GPa and $K_{IC} = 4.4$ MPa $m^{1/2}$.
4. The room temperature flexural strength of the composites was in the range of 620–770 MPa and dependent on the VC content. The maximum strength value was obtained for ZSVC10, while the minimum strength value was observed in ZSVC07.

Acknowledgements

This work was partially supported by a Grant-in Aid C (No. 16K06736) for Scientific Research from the Japan Society for the Promotion of Science (JSPS).

References

[1] Upadhya K, Yang JM, Hoffmann WP (1997) Materials for ultrahigh temperature structural applications. Am Ceram Soc Bull 76:51–56

[2] Wuchina E, Opila E, Opeka M, Fahrenholtz W, Talmy I (2007) UHTCs: ultra-high temperature ceramic materials for extreme environment applications. Interface 16:30–36

[3] Paul A, Jayaseelan DD, Venugopal S, Zapata-Solvas E, Binner J, Vaidhyanathan B, Heaton A, Brown P, Lee WE (2012) UHTS composites for hypersonic applications. Am Ceram Soc Bull 91:22–29

[4] Pastor M (1977) Metallic borides: preparation of solid bodies, sintering methods and properties of solid bodies. In: Matkovich VI (ed) Boron and refractory borides. Springer, New York, pp 457–493

[5] Kuriakose AK, Margrave JL (1964) Oxidation kinetics of zirconium diboride and zirconium carbide at high temperatures. J Electrochem Soc 111:827–831

[6] Tripp WC, Graham HC (1971) Thermogravimetric study of the oxidation of ZrB_2 in the temperature range of 800 to 1500 °C. J Electrochem Soc 118:1195–1199

[7] Monteverde F (2006) Beneficial effects of an ultra-fine α-SiC incorporation on the sinterability and mechanical properties of ZrB_2. Appl Phys A 82:329–337

[8] Zhu S, Fahrenholtz WG, Hilmas GE (2007) Influence of silicon carbide particle size on the microstructure and mechanical properties of zirconium diboride-silicon carbide ceramics. J Eur Ceram Soc 27:2077–2083

[9] Rezaie A, Fahrenholtz WG, Hilmas GE (2007) Effect of hot pressing time and temperature on the microstructure and mechanical properties of ZrB_2–SiC. J Mater Sci 42:2735–2744. https://doi.org/10.1007/s10853-006-1274-2

[10] Ikegami M, Guo SQ, Kagawa Y (2012) Densification behavior and microstructure of spark plasma sintered ZrB_2-based composites wit SiC particles. Ceram Int 38:769–774

[11] Hwang SS, Vasiliev AL, Padture NP (2007) Improved processing and oxidation-resistance of ZrB_2 ultra-high temperature ceramics containing SiC nanodispersoids. Mater Sci Eng A464:216–224

[12] Guo SQ, Yang JM, Tanaka H, Kagawa Y (2008) Effects of thermal exposure on strength of ZrB_2-based composites with nano-sized SiC particles. Compos Sci Technol 68:3033–3040

[13] Tripp WC, Davis HH, Graham HC (1973) Effect of an SiC addition on the oxidation of ZrB_2. Am Ceram Soc Bull 52:612–616

[14] Guo SQ, Nishimura T, Kagawa Y, Tanaka H (2007) Thermal and electric properties in hot-pressed ZrB_2–$MoSi_2$–SiC composites. J Am Ceram Soc 90:2255–2258

[15] Guo SQ, Nishimura T, Mizuguchi T, Kagawa Y (2008) Mechanical properties of hot-pressed ZrB_2–$MoSi_2$–SiC composites. J Eur Ceram Soc 28:1891–1898

[16] Ahmadi Z, Nayebi B, Asl MS, Kakroudi MG (2015) Fractographical characterization of hot pressed and pressureless sintered AlN-doped ZrB_2–SiC composites. Mater Charact 110:77–85

[17] Asl MS, Nayebi B, Ahmadi Z, Pirmohammadi P, Kakroudi MG (2015) Fractographical characterization of hot pressed and pressureless sintered SiAlON-doped ZrB_2–SiC composites. Mater Charact 102:137–145

[18] Zou J, Zhang GJ, Sun SK, Liu HT, Kan YM, Liu JX, Xu CM (2011) ZrO_2 removing reactions of Groups IV–VI transition metal carbides in ZrB_2 based composites. J Eur Ceram Soc 31:421–427

[19] Grigoriev ON, Vinokurov VB, Klimenko LI, Bega ND, Danilenko NI (2016) Sintering of zirconium diboride and phase transformations in the presence of Cr_3C_2. Powder Metall Met Ceram 55:185–194

[20] Zou J, Zhang GJ, Kan YM, Wang PL (2008) Pressureless densification of ZrB_2–SiC composites with vanadium carbide. Scr Mater 59:309–312

[21] Zou J, Zhang GJ, Kan YM, Wang PL (2009) Hot-pressed ZrB_2–SiC ceramics with VC additives: chemical reaction, microstructures, and mechanical properties. J Am Ceram Soc 92:2838–2846

[22] Ma HB, Zou J, Zhu JT, Lu P, Xu FF, Zhang GJ (2017) Thermal and electrical transport in ZrB_2–SiC–WC ceramics up to 1800 °C. Acta Mater 129:159–169

[23] Zou J, Rubio V, Binner J (2017) Thermoability resistance of ZrB_2–SiC–WC ceramics at 2400 °C. Acta Mater 133:293–302

[24] Mendelson MI (1969) Average grain size in polycrystalline ceramics. J Am Ceram Soc 52:443–446

[25] Guo SQ, Hirosaki N, Yamamoto Y, Nishimura T, Mitomo M (2003) Hot-press sintering silicon nitride with Lu_2O_3 addition: elastic moduli and fracture toughness. J Eur Ceram Soc 23:537–545

[26] Anstis GR, Chantikul P, Lawn BR, Marshall DB (1981) A critical evaluation of indentation techniques for measuring fracture toughness. I. Direct crack measurements. J Am Ceram Soc 64:533–538

[27] Monteverde F, Guicciardi S, Bellosi A (2003) Advances in microstructure and mechanical properties of zirconium diboride based ceramics. Mater Sci Eng A346:310–319

[28] Shen Z, Johnsson M, Zhao Z, Nygren M (2002) Spark plasma sintering of alumina. J Am Ceram Soc 85:1921–1927

[29] Sciti D, Silvestroni L, Bellosi A (2006) Fabrication and properties of HfB_2–$MoSi_2$ composites produced by hot pressing and spark plasma sintering. J Mater Res 21:1460–1466

[30] Opeka MM, Takmy IG, Zaykoskl JA (2004) Oxidation-based materials selection for 2000 °C + hypersonic aerosurfaces: theoretical considerations and historical experience. J Mater Sci 39:5887–5904. https://doi.org/10.1023/B:JMSC.0000041686.21788.77

[31] Nayebi B, Asl MS, Kakroudi MG, Farahbakhsh I, Shokouhimehr M (2016) Interfacial phenomena and formation of nano-particles in porous ZrB_2-40 vol% B_4C UHTC. Ceram Int 42:17009–17015

[32] Guo WM, Yang ZG, Zhang GJ (2011) Comparison of ZrB_2–SiC ceramics with Yb_2O_3 additive prepared by hot pressing and spark plasma sintering. Int J Refract Met Hard Mater 29:452–455

[33] Guo WM, Zhang GJ, Zou J, Kan YM, Wang PL (2008) Effect of Yb_2O_3 addition on hot-pressed ZrB_2–SiC ceramics. Adv Eng Mater 10:759–762

[34] Guo SQ, Kagawa Y, Nishimura T, Tanaka H (2008) Elastic properties of spark plasma sintered ZrB_2–ZrC–SiC composites. Ceram Int 34:1811–1817

[35] Chamberlain AL, Fahrenholtz WG, Hilmas GE, Ellerby DT (2004) High-strength zirconium diboride-based ceramics. J Am Ceram Soc 87:1170–1172

[36] Guo SQ, Kagawa Y, Nishimura T, Chung D, Yang JM (2008) Mechanical and physical behavior of spark plasma sintered ZrB_2–ZrC–SiC composites. J Eur Ceram Soc 28:1279–1285